J. Magn. Soc. Jpn., **41**, 46-51 (2017)

<Review>

Control of Magnetization Dynamics in Ordered Alloy Systems

T. Seki[*,**,***], W. Zhou[*], T. Yamamoto[*], and K. Takanashi[*,***]

[*]Institute for Materials Research, Tohoku University, *Sendai 980-8577, Japan*

[**]PRESTO, Japan Science and Technology Agency, *Saitama 322-0012, Japan*

[***]Center for Spintronics Research Network, Tohoku University, *Sendai 980-8577, Japan*

$L1_0$-type alloys and $L2_1$-type Heusler alloys are key materials for future spintronic and magnetic storage devices. $L1_0$-FePt with high uniaxial magnetic anisotropy is a promising material for ultrahigh density recording because of its high thermal stability of magnetization at a nanometer scale. Co-based Heusler alloys showing high spin polarization of conduction electrons enable us to enhance the magnetoresistance effect. In addition, utilizing the magnetization dynamics in these ordered alloys provides us with new paths in the development of spintronic and magnetic storage devices. In this review, we introduce the control of magnetization switching field for $L1_0$-FePt exchange-coupled with $Ni_{81}Fe_{19}$ by utilizing the spin waves in the bilayers, which will be useful for information writing. A nanometer-scaled rf oscillator is also introduced, in which the magnetization dynamics is excited by spin angular momentum transfer. We can improve both the rf output power and the oscillation quality simultaneously by using $Co_2(Fe_{0.4}Mn_{0.6})Si$ Heusler alloy.

Key words: $L1_0$-type ordered alloy, Heusler alloy, magnetization dynamics,

1. Introduction

We introduce our study on "Control of Magnetization Dynamics in Ordered Alloy Systems" in this review paper, which was a research subject of MSJ Outstanding Research Award 2016.

Rapid progress in electronic devices enables us to access various information everywhere, and the accessibility to a large amount of information makes our life comfortable and convenient. Among many kinds of electronic devices, magnetic and spintronic devices play significant roles in data storage technologies. Those devices exploit the direction of magnetization in a small magnet as an information bit, leading to the non-volatile data storage without external power supply. Since ultrahigh density data storage technologies are essential to manage "Big Data", one has highly desired the further development in spintronic and magnetic storage devices. In particular, it is important to simultaneously achieve ultrahigh density storage and ultralow power consumption for the device operation.

In addition to the existing data storage devices mentioned above, various spin-related phenomena have provided new concepts for the development of spintronic devices. For example, magnetization dynamics induced by the torque due to spin angular momentum transfer, which is called spin torque, have recently been found and demonstrated in nano-scaled devices [1]. That has opened a way to give novel functionalities to spintronic devices. From the viewpoint of practical applications, however, the significant improvement of device performance is still required.

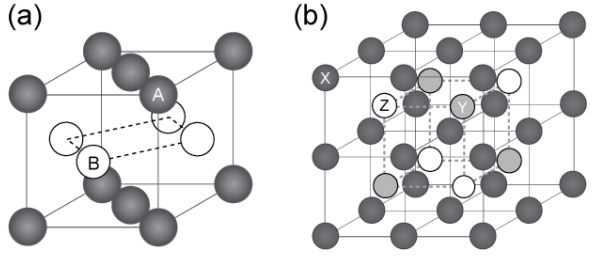

Fig. 1 Schematic illustrations of crystal structures for (a) $L1_0$-ordered and (b) $L2_1$-ordered alloys.

This review paper is devoted to two research subjects: one is the simultaneous achievement of ultrahigh density storage and ultralow power consumption for device operation. The other is the improvement of performance for spin torque devices, especially for a spin torque oscillator (STO) [2]. Key materials for the above research subjects are $L1_0$-type alloys and $L2_1$-type Heusler alloys (Fig. 1), both of which are ordered alloys. In addition to the ordered alloys, the magnetization dynamics is crucial to solve the issues for the magnetic storage and spintronic devices.

2. Spin-wave-assisted magnetization switching in exchange-coupled systems having $L1_0$-FePt

Spintronic and magnetic storage devices face a serious challenge in trying to simultaneously achieve ultrahigh density storage and ultralow power consumption for operation. In order to increase the storage density, the reduction of magnetic bit size is inevitable. A small magnetic volume (V) gives rise to the instability of magnetic information due to the thermal energy (k_BT, k_B is Boltzmann constant and T is temperature). Using a material with high magnetic anisotropy (K) is one of the possible solutions for this problem. However, the high K material leads to another problem, which is the significant increase in the external energy required for the information writing, *i.e.* magnetization switching. This is a dilemma that all the magnetic storage devices possess. A straightforward way to solve this dilemma is

that the switching field of a high K material is reduced only when one needs to switch its magnetization.

$L1_0$-ordered FePt ($L1_0$-FePt) alloy [3] is a representative of high K material, which exhibits the uniaxial magnetic anisotropy (K_u) of 7×10^6 J/m^3 along the c-axis of face-centered tetragonal. Thanks to this high K_u, $L1_0$-FePt is a candidate material for future ultrahigh density magnetic recording media [4]. As discussed above, however, its high K_u also gives rise to the large magnetization switching field (H_{sw}). If the magnetization switching occurs through the coherent rotation of magnetization [5], H_{sw} becomes equal to anisotropy field (H_{ani}). H_{ani} is given by $2\ K_u / M_s$, where M_s is the saturation magnetization. H_{sw} is roughly estimated to be larger than 100 kOe for fully $L1_0$-ordered FePt. Thus, a method to efficiently reduce H_{sw} for $L1_0$-FePt only during the information writing is needed.

A promising method for the efficient H_{sw} reduction is magnetization switching assisted by "external energy" such as microwave energy or thermal energy that are called microwave-assisted switching (MAS) [6,7] and heat-assisted switching [8]. In the case of MAS, microwave is applied to a magnet in order to excite its uniform magnetization precession mode, resulting in the amplification of precession angle followed by the magnetization switching at a low magnetic field. Although this MAS effectively reduces H_{sw}, the excitation frequency for MAS will become close to the sub-THz in case of high K materials such as $L1_0$-FePt because the uniform magnetization precession frequency is proportional to the effective field (H_{eff}) including H_{ani}. From the practical point of view, this high frequency required for MAS is an obstacle to design device structures. Instead of uniform magnetization precession mode, we utilize spin wave modes for an exchange-coupled bilayer system. In the following, we introduce "spin-wave-assisted magnetization switching method" [9-12], which enables us to effectively reduce H_{sw} for $L1_0$-ordered FePt by exciting the spin wave modes in a soft magnetic $Ni_{81}Fe_{19}$ (Permalloy, Py).

Figures 2(a) and 2(b) schematically illustrate the magnetic structures in the exchange-coupled bilayer consisting of the hard magnetic $L1_0$-FePt layer and the soft magnetic Py layer. The $L1_0$-FePt and Py layers are exchange-coupled at the interface, resulting in the magnetic structure where all the magnetic moments are aligned in the same direction. We call this saturated state. When small external magnetic field (H) was applied in the direction opposite to the magnetization vectors, the magnetic moments in Py easily start to rotate because of its low H_{sw}. However, the magnetic moments of Py around the interface are pinned by those of $L1_0$-FePt. As a result, a spatially twisted magnetic structure is formed in the exchange-coupled bilayer, which we call twisted state. In order to experimentally form this twisted magnetic structure, we prepared a

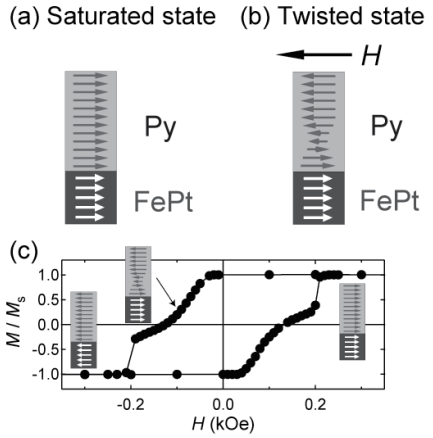

Fig. 2 Schematic illustrations of magnetic structures at (a) saturated state and (b) twisted state for the exchange-coupled bilayer consisting of the hard magnetic $L1_0$-FePt layer and the soft magnetic Py layer. (c) Magnetization curve for the $L1_0$-FePt | Py bilayer under the application of in-plane H [Ref. 11] together with magnetic structures.

thin film on an MgO (110) single crystal substrate using sputtering technique. The stacking of the thin film was MgO Subs. | | Fe (2) | Au (80) | FePt (10) | Py (100) | Au (3) (in nanometer). The FePt layer was grown on the Au buffer at 400 ºC. The substrate heating at 400 ºC promoted the formation of $L1_0$ ordered structure for the FePt layer, leading to the in-plane uniaxial magnetic anisotropy along the in-plane [001] direction. The magnetization curve for the $L1_0$-FePt | Py bilayer is shown in Fig. 2(c) [11], where the magnetization (M) was normalized by the saturated value of M (M_s) and H was applied along the in-plane [001] direction of $L1_0$-FePt. The gradual decrease in M was observed at the low H region. In this H region, the magnetization reversal process was reversible and the spring-back behavior appeared when the minor magnetization curve was measured. This reversible change indicates that the $L1_0$-FePt and the Py are exchange-coupled at the interface and the spatially twisted magnetic structure is formed in the bilayer by applying H.

The ferromagnetic resonance (FMR) spectra for the continuous film of the $L1_0$-FePt | Py bilayer are displayed in Fig. 3(a) [11]. The continuous film was put facedown onto the coplanar waveguide (CPW), and the vector network analyzer FMR technique was employed, where the frequency dependence of S_{11} (defined as the ratio of the reflected voltage to the input voltage) was measured. Three resonance peaks are observed both at H = 200 Oe and H = -200 Oe corresponding to the saturated state and the twisted state, respectively. These peak frequencies (f_0) are plotted as a function of H in Fig. 3(b) [11]. The open circles denote the experimental data whereas the solid curves are the

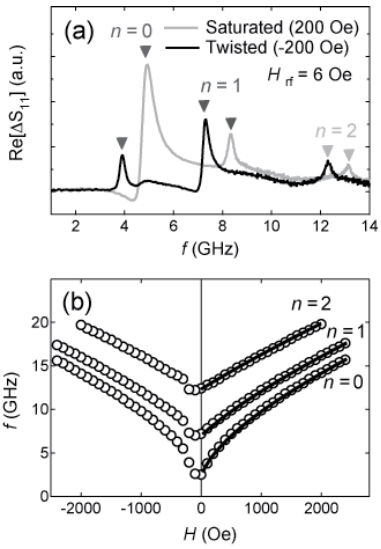

Fig. 3 (a) FMR spectra for the continuous film of the in-plane magnetized $L1_0$-FePt | Py bilayer measured at H = 200 Oe and -200 Oe, which correspond to the saturated and twisted states, respectively. (b) Peak frequencies as a function of H. The open circles denote the experimental data whereas the solid curves are the results of fitting based the analytical model of PSSW mode [Ref. 11].

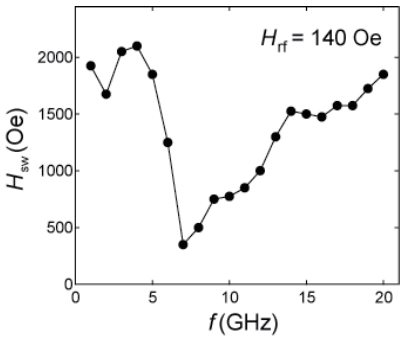

Fig. 4 H_{sw} as a function of excitation frequency for the device with the in-plane magnetized $L1_0$-FePt | Py bilayer. H_{rf} = 140 Oe was applied to the device [Ref. 11].

results of fitting based the analytical model of perpendicular standing spin wave (PSSW) mode [13]. The analytical model of PSSW well explained the dispersion relationship obtained experimentally. In addition to this fact, the numerical simulation suggested that the several PSSW modes with the different number of nodes (n) were mainly excited in the Py layer [9]. For example, n = 0 was the lowest order of the PSSW mode, in which the magnetic moments of Py were pinned at the interface with the hard magnetic $L1_0$-FePt whereas the magnetic moments of Py at the other interface showed the large-amplitude magnetization precession.

We examined the effect of the PSSW excitation on the magnitude of H_{sw} for the microfabricated $L1_0$-FePt | Py bilayer element. The continuous $L1_0$-FePt | Py bilayer was patterned into a rectangular element with dimensions of 2 μm × 50 μm by employing electron beam lithography and Ar ion milling. Figure 4 shows H_{sw} as a function of excitation frequency, where the rf magnetic field (H_{rf}) of 140 Oe was applied [11]. When H_{rf} was not applied, the device showed H_{sw} = 2350 Oe. Below f = 5.0 GHz, no remarkable change in H_{sw} occurred. However, the application of H_{rf} = 6 GHz reduced H_{sw} to 1250 Oe. The largest reduction was observed at f = 7 GHz, in which H_{sw} was obtained to be 350 Oe. This large H_{sw} reduction is attributable to the excitation of PSSW mode. As f was increased from 7 GHz to 20 GHz, H_{sw} increased monotonically. The monotonic increase of H_{sw} with f is the characteristic tendency for the spin wave-assisted switching, which is determined by the dispersion relationship of PSSW modes. In addition to the large H_{sw} reduction, this spin-wave-assisted magnetization switching showed the significant narrow H_{sw} distribution [11]. This narrowing in the H_{sw} distribution suggests that the resonantly amplified spin wave dynamics leads to the reduced H_{sw}. We also studied on the magnetization switching conditions under the spin wave excitation and revealed the limited region of switching condition [14]. This resonant switching behavior suggests that the spin-wave-assisted switching has potential for a selective switching technique in multilevel recording media.

In addition to the case of in-plane magnetized $L1_0$-FePt, we have recently investigated the magnetization dynamics of exchange-coupled bilayers with a perpendicularly magnetized $L1_0$-FePt, where the $L1_0$-FePt layer was epitaxially grown on an MgO (100) single crystal substrate with a Au buffer [12]. In order to examine the effect of magnetization dynamics of the exchange-coupled bilayer on H_{sw} for the perpendicularly magnetized $L1_0$-FePt, we exploited a nanodot consisting of the $L1_0$-FePt layers exchange-coupled with a soft magnetic Py layer having a magnetic vortex. The $L1_0$-FePt layer exhibited H_{sw} = 8.6 kOe without the H_{rf} application. When H_{rf} = 200 Oe with f = 11 GHz was applied, H_{sw} was reduced from 8.6 kOe to 2.8 kOe. By comparing the experimental result with the micromagnetic simulation, we found that the vortex dynamics of azimuthal spin waves in Py effectively triggered the reversed-domain nucleation in $L1_0$-FePt at a low H. This demonstrates that the excitation of spin wave leads to the efficient H_{sw} reduction even for the exchange-coupled system with the perpendicularly magnetized $L1_0$-FePt.

Although the excitation of spin wave dynamics in the exchange-coupled systems is useful to reduce H_{sw}, the present bilayer structures having the soft magnetic layer may lead to the degradation of thermal stability of magnetization compared with an $L1_0$-FePt single layer film. The evaluation of thermal stability for the

exchange-coupled bilayer will be an issue to be addressed in future.

3. Spin torque oscillator using Co-based Heusler alloy

Apart from the issue for ultrahigh density storage discussed in the previous Section, we also need to open up a way for new device applications for the further progress in the spintronics research field. In other words, we should provide spintronic devices with novel functionalities to realize a diversity of applications. An emerging spintronic device is STO [2], which is a nanometer-scaled rf oscillator, *e.g.* for on-chip communications or radar. The key physical phenomenon to operate the STO is the spin torque-induced magnetization dynamics. An STO consists of a layered structure of a ferromagnetic (F1) layer | a nonmagnetic (N) metal (or an insulator (I)) | another ferromagnetic (F2) layer. In case that we inject the electric current from F2 to F1, the conduction electrons are spin-polarized by the F1 layer (a spin polarizer), which exerts spin torque on the local magnetic moments of the F2 layer (a free layer). When the spin torque and the intrinsic damping torque are balanced in the F2 layer, the magnetization shows the self-sustained precession motion around H_{eff}. For current-perpendicular-to-plane (CPP) giant magnetoresistance (GMR) devices with F1 | N | F2 and magnetic tunnel junctions (MTJs) with F1 | I | F2, this steady magnetization precession produces a change in the device resistance via the GMR effect and the tunnel magnetoresistance effect, respectively [15-17]. Since a dc electric current (I_{dc}) is applied to the device, the time-dependent device resistance ($R(t)$) is converted into rf voltage (V_{rf}). Consequently, the device emits rf output power (P_{out}). This is the central mechanism of the STO, and its simple architecture composed of a single nanometer-scaled element is one of the attractive aspects of the STO.

However, the STOs have several crucial issues that need to be solved before the practical use: (i) the enhancement of P_{out}, (ii) improvement of the rf oscillation quality, and (iii) increasing the frequency tunability by an electric current and/or a magnetic field. MTJ-based STOs with an MgO tunnel barrier may solve the first issue since the P_{out} is roughly proportional to the square of the MR ratio. However, MTJ-based STOs have other problems, which are a wide oscillation linewidth observed generally [17], the risk of the dielectric breakdown of the tunnel barrier under large bias voltages [18], and the non-negligible shot noise due to the existence of tunnel barrier. On the other hand, a CPP-GMR device generally exhibits a narrow oscillation linewidth compared with the MTJ-based STOs [19]. Furthermore, a CPP-GMR stack is free from the risk of dielectric breakdown of a tunnel barrier material, and has the negligible contribution of shot noise. Thus, if the CPP-GMR effect can be enhanced, it could be a candidate of a high performance STO. One promising

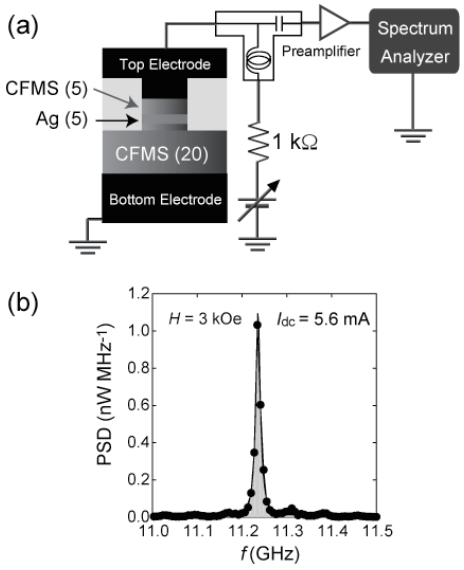

Fig. 5 (a) Schematic illustration of CPP-GMR device having CFMS | Ag | CFMS layers together with the measurement setup for rf oscillation properties, and (b) its rf spectrum at perpendicular H = 3 kOe and I_{dc} = 5.6 mA. The CPP nanopillar has an ellipsoidal shape of 0.1 × 0.17 μm^2. [Ref. 25]

way to enhance the MR ratio in a CPP-GMR device is to use half metallic ferromagnets showing the full spin-polarization of conduction electrons, in which the density of states at the Fermi level exists only in one spin channel.

Co_2MnSi (CMS) is one of the Co-based Heusler alloys theoretically predicted as a half metal [20] and showing high GMR ratio experimentally [21], leading to the enhancement of P_{out} even for a CPP-GMR-based STO. We reported that the large P_{out} = 1.1 nW was achieved for the CPP-GMR device with the CMS | Ag | CMS stack [22,23]. $Co_2Fe_{0.4}Mn_{0.6}Si$ (CFMS) is another full-Heusler alloy exhibiting high spin polarization of conduction electrons. In fact, the CPP-GMR devices with CFMS | Ag | CFMS showed the MR ratios larger than CMS | Ag | CMS [24]. Thus, CFMS is also a candidate material for developing high performance STO [25,26].

Figure 5(a) depicts a structure of the CPP-GMR having CFMS layers and the measurement setup to electrically detect the spin torque-induced magnetization dynamics. A stacking structure of Cr (20 nm) | Ag (40 nm) | CFMS (20 nm) | Ag (5 nm) | CFMS (3 nm) | Ag (2 nm) | Au (5 nm) was prepared on an MgO (100) single crystal substrate using an ultrahigh-vacuum magnetron sputtering system. The 20 nm-thick bottom CFMS and the 3 nm-thick top CFMS layers were grown at room temperature followed by *in-situ* annealing at 500ºC to promote the chemical ordering. The film was patterned into a CPP nanopillar with an ellipsoidal shape (0.1 × 0.17 μm^2). The top and the bottom CFMS layers for the

present device behave as the free layer and the fixed layer, respectively, against spin torque. The CPP-GMR device was connected to the circuit with a two-terminal rf probe and I_{dc} was applied through a bias-Tee. Positive I_{dc} is defined as the direction, in which electrons flow from the upper to the lower CFMS layer. The output V_{rf} was amplified by a preamplifier and was monitored in frequency-domain by a spectrum analyzer.

In order to understand the H direction dependence of oscillation properties, we measured the spin torque oscillation both under the in-plane and the perpendicular H. When in-plane H and I_{dc} were applied to the device along the long-axis of ellipsoidal pillar, the peak appeared in the power spectral density. However, the small P_{out} (0.03 nW) was obtained and a wide oscillation linewidth (Δf) of 76 MHz was observed, which were attributable to the inhomogeneous effective magnetic field (H_{eff}). In contrast to the spin torque oscillation under the in-plane H, we considerably improved the oscillation properties by applying the perpendicular H. Figure 5(b) displays an rf spectrum at

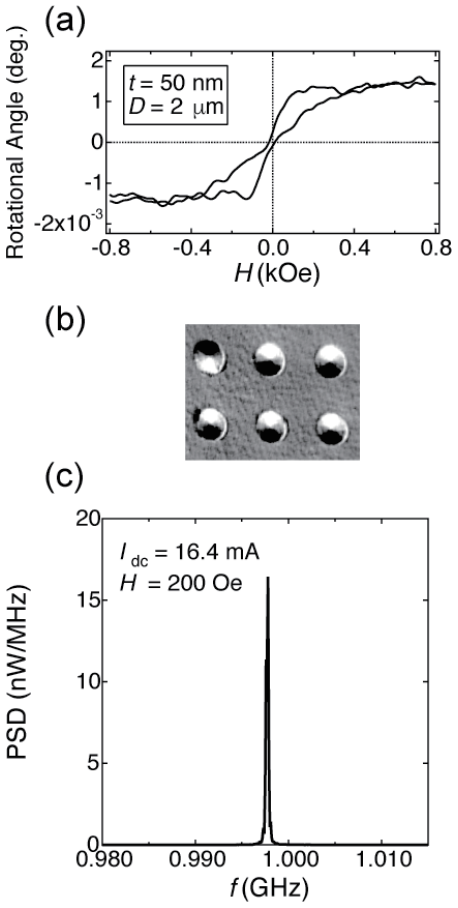

Fig. 6 (a) L-MOKE loop and (b) magnetic domain image at the remanence observed using PEEM-XMCD for the CFMS disks with the diameter of 2 μm and the thickness of 50 nm. [Ref. 28] (c) rf spectrum for the CPP-GMR device having the magnetic vortex in the CFMS layer.

H = 3 kOe and I_{dc} = 5.6 mA [25]. The I_{dc} dependence of oscillation frequency (f_0) showed the blue shift against I_{dc}, suggesting that the perpendicular H led to an out-of-plane mode of magnetization precession. The maximum value of P_{out} was obtained to be 23.7 nW together with the narrow Δf = 10 MHz. This P_{out} was much larger than those reported in the CPP-GMR devices using conventional ferromagnetic layers, and was one order of magnitude smaller than the performance of the previous MTJ-based STO showing P_{out} = 0.14 μW [17]. We also performed the micromagnetic simulation to reveal the detail of magnetization dynamics [25]. Although we successfully achieved the large P_{out} by using the highly spin-polarized CFMS, the simulated results suggested the formation of spatially non-uniform magnetic structure during the spin torque oscillation and the large incoherency in the precession trajectory. This implies that the improvement of coherency in the spin torque oscillation enables us to further enhance P_{out}.

One of the possible ways to improve the coherency of spin torque oscillation is to utilize the dynamics of magnetic vortex. A study on the vortex STO reported the narrow Δf, leading to the high Q factor (Δf / f_0) [27], which is owing to the stable vortex oscillation. The stability of vortex oscillation originates from the topologically stable magnetic structure and good consistency of the magnetization distribution with the spatial distribution of the Oersted field formed by the dc current. Thus, we examined the formation of magnetic vortex and the control of vortex dynamics in the CFMS nanodisk, in which the CFMS layers were epitaxially grown on the MgO substrate. Figures 6(a) and 6(b) show the longitudinal magneto-optical Kerr effect (L-MOKE) loop and the magnetic domain image at the remanence observed using a photoemission electron microscope with X-ray magnetic circular dichroism (PEEM-XMCD), respectively, for the circular CFMS disks with the diameter of 2 μm and the thickness of 50 nm [28]. The shape of L-MOKE loop with low remanent magnetization was attributed to the magnetization process undergoing the formation of magnetic vortex. In addition, the curling in-plane magnetic moments were clearly observed in the magnetic domain image. Consequently, one sees that the magnetic vortex can be stably formed even in the epitaxially grown CFMS disks. Then, we fabricated the STO with the CFMS disk with a diameter of 240 nm, in which the magnetic vortex was formed in the CFMS disk [29]. The STO was made of the stack of MgO (100) Subs. | | Cr (20 nm) | Ag (20 nm) | CFMS (20 nm) | Ag (5 nm) | CFMS (30 nm) | Ag (2 nm) | Au (3 nm), in which 30 nm-thick CFMS was patterned into the disk shape to stabilize the magnetic vortex. Figure 6(c) shows an rf spectrum for the CPP-GMR device having the magnetic vortex in the CFMS layer. The sub-GHz oscillation with a narrow oscillation linewidth (Δf = 0.4 MHz) was observed, which originated from the vortex dynamics. From the

systematic study on the oscillation properties for vortex STO with CFMS, we found that the high P_{out} > 10 nW and the high Q factor > 5000 were achieved simultaneously at an optimum condition [29]. Our experimental results indicate that the utilization of vortex dynamics in CFMS is a promising way to provide a significant improvement of the performance of STOs.

4. Summary

In this review, we introduced two research topics: spin-wave-assisted magnetization switching in the bilayers with $L1_0$-FePt and Py, and high performance STOs using the CFMS Heusler alloy.

For the in-plane and perpendicularly magnetized configurations of $L1_0$-FePt layers, we successfully reduced H_{sw} for $L1_0$-FePt utilizing the spin waves in the bilayers. We expect that this spin-wave-assisted magnetization switching will be used as an information writing technique of future magnetic storage devices.

The STOs having the CFMS layers were developed, and both the P_{out} and the Q factor were improved by exploiting the highly spin-polarization of CFMS Heusler alloy and the dynamics of magnetic vortex. We believe that vortex STO with CFMS serves as a key for the further progress in spintronic devices.

Acknowledgements These works are partly in collaboration with Dr. H. Imamura, Dr. H. Arai and Dr. T. Yamaji (AIST), Prof. Y. Nozaki (Keio Univ.), Prof. M. Mizuguchi, Prof. T. Kubota, Dr. H. Yako (Tohoku Univ.), Dr. Y. Sakuraba (NIMS), and Prof. M. Kotsugi (Tokyo Univ. of Sci.). We also thank Dr. T. Ohkochi (SPring-8) and Mr. Y. Murakami and Mr. I. Narita (Tohoku Univ.) for their technical assistance. These works were partially supported by a Grant-in-Aid for Young Scientists A (25709056), Grant-in-Aid for Scientific Research S (23226001), Grant-in-Aid for Scientific Research B (16H04487), Institute for Division For Interdisciplinary Advanced Research and Education, Tohoku Univ. and the Japan Society for the Promotion Science Research Fellowship for Young Scientist. The device fabrication and the structural characterization were partly performed at Cooperative Research and Development Center for Advanced Materials, IMR, Tohoku University.

References

1) Brataas, A. D. Kent, and H. Ohno: *Nature Mater.* 11, 372 (2012).
2) D. C. Ralph and M. D. Stiles: *J. Magn. Magn. Mater.* 320, 1190 (2008).
3) O. A. Ivanov, L. V. Solina, V. A. Demshina, and L. M. Magat: *Phys. Met. Metallogr.* 35, 81 (1973).
4) D. Weller, A. Moser, L. Folks, M. E. Best, W. Lee, M. F. Toney, M. Schwickert, J. U. Thiele, and M. F. Doerner. *IEEE Trans. Magn.* 36, 10 (2000)
5) E. C. Stoner and E. P. Wohlfarth: *Nature* 160**,** 650 (1947)
6) J.-G. Zhu, X. Zhu, and Y. Tang: *IEEE Trans. Magn.* 44, 125 (2008).
7) S. Okamoto, N. Kikuchi, M. Furuta, O. Kitakami, and T. Shimatsu: *J. Phys. D: Appl. Phys.* 48, 353001 (2015).
8) D. Atkinson and R. P. Cowburn: *Appl. Phys. Lett.* **85**, 1386 (2009).
9) T. Seki, K. Utsumiya, Y. Nozaki, H. Imamura, and K. Takanashi: *Nature Comm.,* 4, 1726 (2013).
10) T. Seki, K. Hotta, H. Imamura, Y. Nozaki, and K. Takanashi: *Appl. Phys. Lett.* 103, 122403 (2013).
11) T. Seki, W. Zhou, and K. Takanashi: *J. Phys. D: Appl. Phys.* 49, 075002 (2016).
12) W. Zhou, T. Seki, H. Arai, H. Imamura, and K. Takanashi: *Phys. Rev. B* 94, 220401(R) (2016).
13) S. O. Demokritov, B. Hillebrands, and A. N. Slavin: *Phys. Reports* 348, 441 (2001).
14) W. Zhou, T. Yamaji, T. Seki, H. Imamura, and K. Takanashi: *Appl. Phys. Lett.* (Accepted).
15) S. I. Kiselev, J. C. Sankey, I. N. Krivorotov, N. C. Emley, R. J. Schoelkopf, R. A. Buhrman, and D. C. Ralph: *Nature* 425, 380 (2003).
16) W. H. Rippard, M. R. Pufall, S. Kaka, S. E. Russek, and T. J. Silva: *Phys. Rev. Lett.* 92 027201 (2004).
17) A. M. Deac, A. Fukushima, H. Kubota, H. Maehara, Y. Suzuki, S. Yuasa, Y. Nagamine, K. Tsunekawa, D. D. Djayaprawira, and N. Watanabe: *Nature Phys.* 4, 803 (2008).
18) D. Houssameddine, S. H. Florez, J. A. Katine, J.-P. Michel, U. Ebels, D. Mauri, O. Ozatay, B. Delaet, B. Viala, L. Folks, B. D. Terris, and M.-C. Cyrille: *Appl. Phys. Lett.* 93, 022505 (2008).
19) Q. Mistral, J.-V. Kim, T. Devolder, P. Crozat, C. Chappert, J. A. Katine, M. J. Carey, and K. Ito: *Appl. Phys. Lett.* 88, 192507 (2006).
20) S. Ishida, S. Asano, and J. Ishida: *J. Phys. Soc. Jpn.*, 53, 2718 (1984).
21) Y. Sakuraba, K. Izumi, Y. Miura, K. Fuasukawa, T. Iwase, S. Bosu, K. Saito, K. Abe, M. Shirai, and K. Takanashi: *Phys. Rev. B* **82**, 094444 (2010).
22) R. Okura, Y. Sakuraba, T. Seki, K. Izumi, M. Mizuguchi, and K. Takanashi: *Appl. Phys. Lett.*, 99, 052510 (2011).
23) T. Seki, Y. Sakuraba, R. Okura, and K. Takanashi: *J. Appl. Phys.* 113, 033907 (2013).
24) Y. Sakuraba, M. Ueda, Y. Miura, K. Sato, S. Bosu, K. Saito, M. Shirai, T.J. Konno, and K. Takanashi: *Appl. Phys. Lett.* 101, 252408 (2012).
25) T. Seki, Y. Sakuraba, H. Arai, M. Ueda, R. Okura, H. Imamura, and K. Takanashi: *Appl. Phys. Lett.* 105, 092406 (2014).
26) T. Yamamoto, T. Seki, T. Kubota, H. Yako, and K. Takanashi: *Appl. Phys. Lett.* 106, 092406 (2015).
27) V. S. Pribiag, I. N. Krivorotov, G. D. Fuchs, P. M. Braganca, O. Ozatay, J. C. Sankey, D. C. Ralph, and R. A. Buhrman: *Nature Phys.* 3 498-503 (2007).
28) T. Yamamoto, T. Seki, M. Kotsugi, and K. Takanashi: *Appl. Phys. Lett.* 108, 152402 (2016).
29) T. Yamamoto, T. Seki, and K. Takanashi: *Phys. Rev. B* 94, 094419 (2016).

Received Feb. 08, 2017; Accepted Mar. 08, 2017